JOURNAL OF CATALYSIS 141, 510–523 (1993)

Vanadium Effects on Pillared Rectorite Catalysts

M. L. OCCELLI,* J. M. DOMINGUEZ,† AND H. ECKERT‡

*Zeolites and Clays Program, MST Laboratory, Georgia Tech Research Institute, Atlanta, Georgia 30332-0800; †IMP, Eje Central, L. Cardenas N152, Mexico D.F., Mexico; and ‡Department of Chemistry, University of California, Santa Barbara, Goleta, California

Received July 22, 1992; revised December 18, 1992

Energy dispersive spectroscopy (EDS), microprobe analysis, X-ray diffraction (XRD), high-resolution electron microscopy (HREM), and ^{51}V solid-state NMR, together with microactivity test (MAT) measurements, have been used to characterize the effects that V-impurities have on the physiochemical properties of a sample of natural rectorite pillared with alumina clusters. Results indicate that although V initially is preferentially located in the pillared clay micropores, after calcination or steaming it migrates, generating clay platelets with a V-enriched surface. During thermal treatment in the presence of 0.5–1.0% V, minor changes in the clay-pillared structure are observed by XRD or HREM. However, at hydrothermal conditions, 1% V causes pillar decomposition and a collapse of the clay microporous structure that result in a loss of surface area, basal spacing, and catalytic activity for gas-oil cracking. HREM data show that steaming in the presence of 1% V generates wavy and misoriented planes; however, in contrast to montmorillonites, the collapsed rectorite partially retains its face-to-face stacking of silicate layers. These processes are conveniently monitored by ^{51}V solid-state NMR, which is capable of distinguishing the various coordination environments in which V can be found after thermal and hydrothermal treatments.

INTRODUCTION

Rectorite, when pillared with polyoxocations of Al or Zr, can form microporous solids that, in contrast to similarly prepared pillared montmorillonites, have thermal and hydrothermal stability comparable to that exhibited by zeolite-containing fluid-cracking catalysts (FCC) (*1–3*). In fact, after steam-aging (760°C/5 h, 100% steam, 1 atm) a Mg-rectorite sample pillared with Al_2O_3-clusters has (at microactivity test conditions) cracking activity and gasoline selectivity similar to that of a commercially available FCC (*3*). Like pillared montmorillonites, pillared rectorites offer less slurry oil (SO) generation together with greater light-cycle gas-oil (LCGO) selectivity; however, their coke generation remains high (*3*).

During the cracking of V-contaminated crudes, FCCs irreversibly lose their cracking activity owing to the destructive interactions that occur during catalyst regeneration between V contaminants and the zeolite present in the FCC matrix. With HY-type zeolite, the structural collapse generates mullite, together with minor amounts of tridymite and an X-ray amorphous V_2O_5-like phase (*4*). With calcined rare earth exchanged Y (CREY), the collapse of the faujasite structure occurs with $REVO_4$ formation (*4*). Vanadium–zeolite interactions have been reviewed in a recent article (*4*). It is the purpose of this paper to examine and report the effects that V contaminants have on a sample of Mg–rectorite pillared with Al_2O_3-clusters.

EXPERIMENTAL

A natural rectorite sample from Garland County, Arkansas, was obtained from the Clay Mineral Society Repository. The sample consists of quartz aggregates containing 10–20% rectorite from which the clay was separated using ultrasonification, sedimen-

0021-9517/93 $5.00

tation, and flocculation treatments described in detail elsewhere (*3*). The rectorite thus obtained contained only trace amounts of quartz and kaolinite impurities and after drying (400°C/2 h) *in vacuo* had a BET surface area of only 10.4 m^2/g. This Mg–rectorite contained 3.89% Na_2O (nonexchangeable), 35.5% Al_2O_3, 49.4% SiO_2, and 0.80% Fe_2O (*3*).

The clay was expanded by reacting a slurry containing 0.0075 g clay/g water with an excess of aluminum chlorohydroxide (ACH, Chlorhydrol from the Reheis Chemical Company). All powder diffraction measurements were obtained with a Siemens D-500 diffractometer at a CuK_α scan rate of 1°/min using monochromatic CuK_α radiation. Samples were prepared as standardized specimens by placing 0.08 g of clay on a glass slide 27 mm × 46 mm in size. A few drops of butanol were then added to form a clay slurry that could be evenly spread on the slide. The same specimen holder was used to avoid apparent *d*-spacing variations resulting from differences in sample thickness.

A solution of vanadyl naphthenate in toluene was used to metal-load pillared rectorite samples according to an established procedure (*6*). The naphthenate solution was obtained from Pfaltz and Bauer, Inc., and contained 2.9 wt% V. The decomposition of the naphthenate was accomplished by heating in air at 540°C/10 h. Steam-aging was then performed by passing steam at 760°C over the catalysts for 5 h. Calcined and steam-aged samples were allowed to rehydrate at room temperature in air.

NMR experiments were undertaken at 79.0 MHz on a General Electric GN-300 spectrometer, equipped with a probe from Doty Scientific and an Explorer fast digitizer. Experiments were run under static conditions using the following typical experimental parameters: 10° pulses of 1 μs length, 1 s recycle delays, 4 K data points. The dead time between pulse and spectrum acquisition was 10 μs; typically, 30,000 to 40,000 scans were acquired. Although the spectra observed with the simple one-pulse sequence might be somewhat distorted, this method is preferred here over spin echo techniques, which are affected more by differences in excitation selectivity for various lineshape components with different nutation behaviors. All spectra were processed with an exponential line-broadening function (typically 100–500 Hz) prior to FT. The chemical shifts are reported relative to liquid $VOCl_3$. ^{29}Si MASNMR studies (performed routinely on all samples) indicated that V did not affect silicon coordination.

High-resolution electron microscopy (HREM) data was obtained using a JEOL-2000 instrument at 200 KV by including at least two rings plus the basal reflections into the objective aperture. Rectorite flakes were imaged at about 3×10^5 magnification power. The optimal orientation along [001] or [010] was verified by the appearance of the (020) or other crossed planes. Interlayer distances were measured by calibration with graphite-type standards (i.e., d = 3.34 Å), while electron diffraction patterns were measured through the use of gold films.

Microanalysis of the V-contaminated clay samples was performed using a JEOL-100CX machine fitted with a Tracor Northern-5500 system analyzer. A typical microregion was about 200 Å in diameter for point analysis, or 0.5 μm for the other cases. Compositional analysis of the individual rectorite crystals was performed in the electron microscope by exciting the sample region with an electron beam (of 200 Å at 40 keV, 120 s) and then by recording the characteristic X-rays of the elements present on the sample surface. Energy-dispersive spectroscopy (EDS) analysis was performed using a very fine probe (200 Å in diameter) with a penetration of about 0.1 μm from the clay crystal surface.

Catalyst evaluation was performed with a microactivity test (MAT) using conditions described elsewhere (*7*). Conversions are on a vol% fresh-feed (FF) basis and have been defined as $[V_f\text{-}V_p/V_f] \times 100$, where V_f

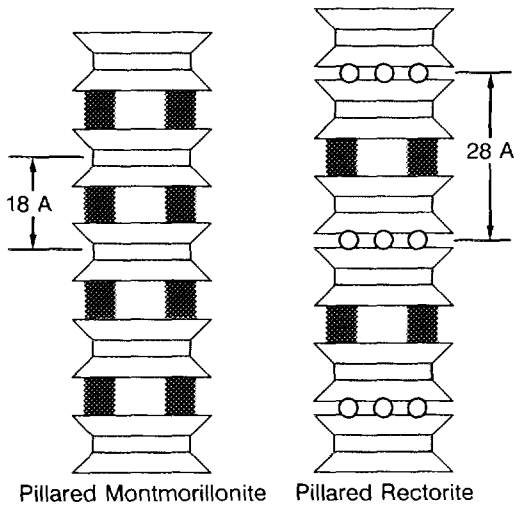

FIG. 1. Schematic representation of two pillared clay catalysts. The T–O–T 3-layers sequence (T = tetrahedral, 0 = octahedral) in rectorite and montmorillonite is represented by trapezoids and rectangles. Exchange of charge compensating cations with Al_{13}-ions expand the silicate layers and after calcination the bulky oxycations form pillars. In montmorillonite, the interlamellar space available to sorption and catalysis is separated by one silicate layer, in rectorite by two.

is the volume of feed and V_p is the volume of product with b.p. > 204°C.

RESULTS AND DISCUSSION

Rectorite is a mixed-layer clay consisting of a regular intrastratification of low-charge-density, montmorillonite-like layers and high-charge-density (nonexpandable) mica-like layers. The charge-compensating cations in the swelling layers can be easily replaced with large $[Al_{13}O_4(OH)_{24}(H_2O)_{12}]^{+7}$ ions that, once introduced, prop apart the platelets of the montmorillonite-like layers; see Fig. 1. When this occurs, the rectorite $d(001)$ spacing shifts from 24.1 to 28.7 Å (Figs. 2A and 2B) and the clay surface area increases moderately to 180 m^2/g. Typically, well-pillared montmorillonites have BET surface area in the 300–400 m^2/g range. If only half of the silicate layers can be expanded (as in the case of a regularly intrastratified rectorite), then surface area values in the 150–200 m^2/range are to be expected for a well-pillared rectorite sample free of major phase impurities; see Fig. 2A.

After drying and calcination at 400°C/2 h in air, the partial dehydroxylation of the Al_{13}-pillars reduces the $d(001)$ spacing to 28.0 Å, a value well in agreement with the sum of the thickness of the mica layer (9.6–10 Å) and the thickness of the calcined pillared montmorillonite layer (17.5–18.5 Å) (*3*). Calcination (at 800°C/5 h, air) or steaming (760°C/5 h, 100% steam, 1.0 atm) reduces the clay surface area to 147 m^2/g and further decreases the $d(001)$ spacing to 26.5 Å. However, the intensity, as well as the sharpness of the 001 reflection, is retained, indicating that this severe thermal treatment has little effect on the clay-pillared structure. Thermal analysis data (*3*) has indicated that at 1000°C/air the parent rectorite collapses with formation of quartz. The pillared product (ACH–rectorite) collapses instead (at 1000°C/air) forming, in addition to quartz, mullite together with minor amounts of δ-alumina. Steaming (at 760°C/5 h) ACH–rectorite samples containing 0.5–1.0% V did not induce the formation of new phases.

Pillared rectorites contain both Brønsted and Lewis acid sites; their strength and density is somewhat lower than those observed in pillared montmorillonites (*3*). When cracking gas oil at microactivity test (MAT) conditions, steam-aged pillared rectorites have high cracking activity and exhibit selectivity properties typical of pillared clays; their coke make is 60–65% higher than in a commercial FCC (*3*); see Table 1.

After loading 0.5–1.0% V (using a solution of vanadyl napthenate in benzene) and calcination at 540°C/10 h air, the clay retains most of its surface area and pillared structure. With 0.5% V, after steaming this ACH–rectorite lost 31% of its surface area while retaining 81% of its initial cracking activity. By comparison, a similarly steam-aged and zeolite-rich FCC such as Davison's GRZ-1 (containing ~35% calcined rare earth exchanged Zeolite Y,CREY) with

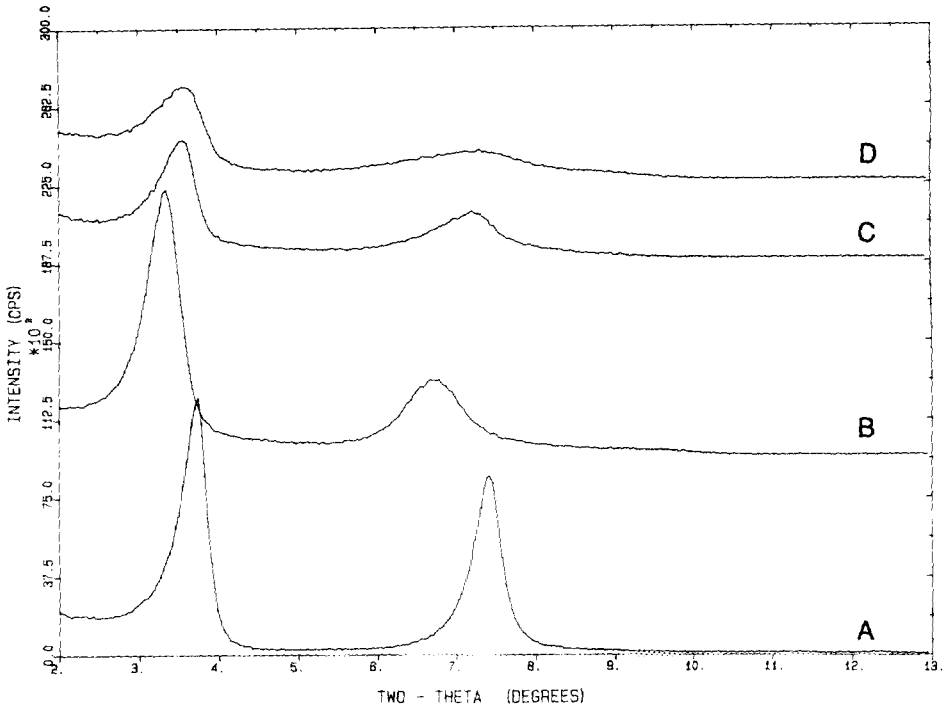

FIG. 2. X-ray diffractograms of a sample of Mg–rectorite (A) before and after pillaring with alumina clusters, followed by (B) calcination at 540°C/10 h in air and steaming at 760°C/5 h in the presence of (C) 0.5% V, and (D) 1.0% V.

0.5% V retained 87% of it is initial activity. Both catalysts lose their useful cracking activity at 1% V. In fact, steaming in the presence of V causes the pillars to decrease in size, and with 1.0% V, the clay surface area and $d(001)$ spacing decreased to 18 m^2/g and 24.6 Å from 147 m^2/g and 26.2 Å, respectively (see Figs. 2C and 2D). The diffraction lines near 24.6 and 14.7 Å in Figs. 2C and 2D indicate that V, at hydrothermal conditions, decomposes the pillars while partially retaining the face-to-face stacking of the clay silicate layers.

Microanalysis Results

Samples were analyzed by means of energy dispersive spectroscopy (EDS) methods in the microscope (at 40 KeV, 120 s),

TABLE 1

Microactivity Test Results for a Steam-Aged Sample of ACH–Rectorite before and after Loading with 0.5% V and 1.0% V (*7*)

% V	Conversion (V% FF)	Gasoline (V% FF)	LCGO (V% FF)	SO (V% FF)	Coke (wt% FF)	SA (m^2/g)
0.0	85.2	59.5	13.2	1.6	10.2	147
0.5	69.2	51.6	23.5	7.3	8.0	101
1.0	20.3	7.6	19.2	60.5	3.0	18

TABLE 2

Elemental Analysis of a Sample of Mg–Rectorite before and after Pillaring with Al_{13}-clusters and Loading with 0.5 or 1.0% Vanadium (C = Calcined at 540°C/10 h Air; S = Steamed at 760°C/5 h).

	AA (wt%)				EDS (wt%)			
	%V	%Fe	%Al	%Si	%V	%Fe	%Al	%Si
Mg–Rectorite	0.0	0.55	18.8	23.1	0.0	3.6	18.1	22.8
ACH–Rectorite, C	0.0	0.48	21.4	23.6	0.0	3.4	21.9	19.0
ACH–Rectorite, S	0.0	0.48	21.4	23.6	0.0	1.4	19.1	23.7
ACH–Rectorite, C	0.5	0.48	21.4	23.6	1.1	1.2	18.2	22.9
ACH–Rectorite, S	0.5	0.48	21.4	23.6	2.6	2.4	18.8	21.6
ACH–Rectorite, C	1.0	0.48	21.4	23.6	3.0	2.8	17.4	20.1
ACH–Rectorite, S	1.0	0.48	21.4	23.6	3.6	3.9	17.0	20.1

using a broad beam for average analysis and a narrow beam for point analysis. The broad beam was about 10 μm in diameter and the finer probe was about 0.02 μm. The large difference observed when V (and Fe) concentration is measured by AA and by EDS indicate that most of these elements are preferentially located near or on the clay platelets surface (see Table 2). Although AA and EDS measure similar Si concentration in the parent rectorite, EDS gives lower Si values than AA in the pillared samples as shown in Table 2. It is believed that the presence of bulky Al_{13}-clusters in the clay silicate layers prevent the accurate detection of all of the Si present near or on the clay crystal surfaces. After steaming, Al and Fe migrate. Thus, the steam-aged (V-free) pillared rectorite Si/Al molar ratio for the crystal surface increases to 1.16 from 0.81, a value observed in the parent Mg-rectorite; see Table 2.

Results in Tables 2 and 3 indicate that following the oxidative decomposition (at 540°C/10 h in air) of the VO^{+2}–naphthenate, some vanadium migrates from the pillared clay microspace onto its surface. Steaming promotes further V (and Fe) migration and a concentration gradient is established between the crystal rims and its face (see Table 3). Furthermore, at 0.5% V, steaming seems to cause an Al-enrichment at the crystal rims (see Table 3). When the V-loading is increased to 1.0% V, a depletion of Al from the rims occur and the Al concentration on the crystal face decreases to 17.0 from 18.8%, see Table 3. Thus, it is believed that the hydrolysis of V-compounds during

TABLE 3

EDS Analysis of Rims (R) and (001) Face (F) of ACH–Rectorite Crystals Loaded with V after Calcination and Steaming.

wt%	0.5% Vanadium				1.0% Vanadium			
	Calcined		Steamed		Calcined		Steamed	
	R	F	R	F	R	F	R	F
Si	22.8	22.9	22.1	21.6	20.1	20.1	20.1	20.1
Al	18.0	18.2	19.6	18.8	17.0	17.4	16.0	17.0
Fe	1.5	1.2	2.0	2.4	2.0	2.8	2.4	3.9
V	1.2	1.1	1.4	2.6	2.3	3.0	2.2	3.6

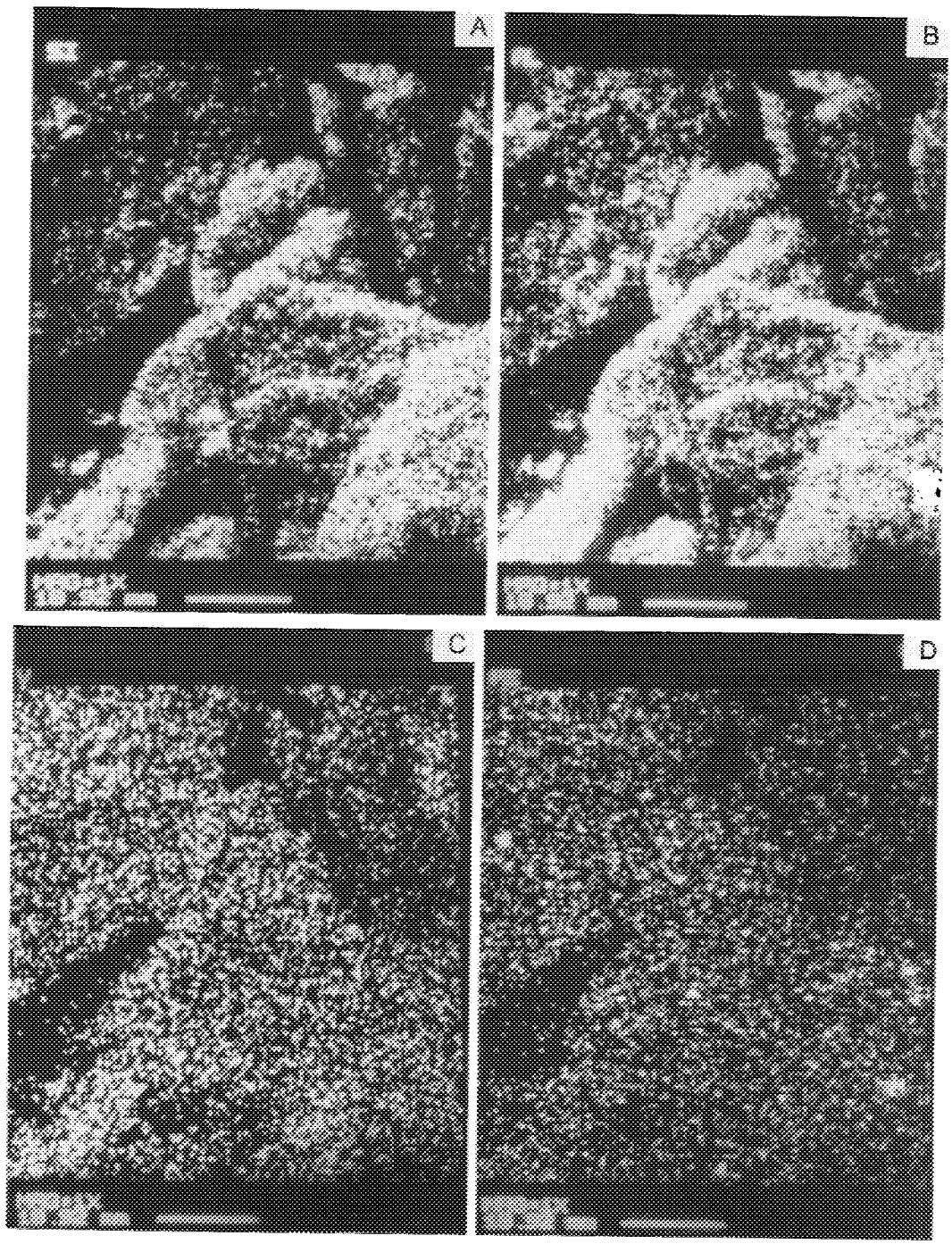

FIG. 3. X-ray maps of the distribution of (A) Si, (B) Al, (C) V, and (D) Fe on the calcined rectorite 001 surface.

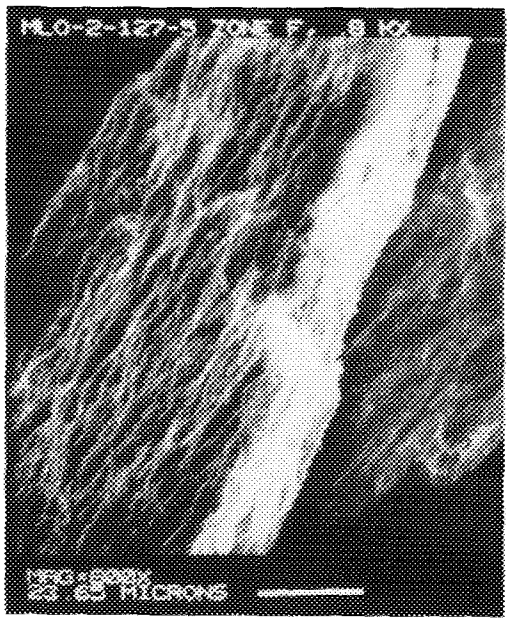

FIG. 4. TEM photomicrograph of a rectorite plate. The clay sample has been loaded with 1.0% V and steam-aged.

steaming at 760°C generates acids (*4*) that decompose the Al_{13}-clusters (pillars) into alumina fragments that are then expelled from the clay pillared structure.

Point analysis data have indicated the presence of V levels two or three times higher than the average region composition data reported above, suggesting the formation of V and Fe islands. Furthermore, V and Fe have similar concentration profile across the clay platelets, indicating a close association between these two elements.

Morphology and X-ray maps of the ACH–rectorite sample loaded with 1% V are shown in Figs. 3 and 4. The samples examined consist of plates 400 × 800 μm in size; smaller crystals were also present. The X-ray maps in Figs. 3A and 3B show the existence of a correlation between Si and Al and that their distribution follows the plate contour, indicating a close association of these two elements with the clay structure. In agreement with EDS data, Al maps are more intense than Si maps, owing to the existence of an Al-enriched clay surface. Furthermore, X-ray maps show that V and Fe are well distributed on the clay surface and that their presence extends beyond the platelets contour (see Figs. 3C and 3D). Small aggregates, or islands, of V and Fe are present and some rims appear richer in V than the extended crystal surface. X-ray maps (not shown) of Si, Al, and Fe have their intensity reduced by the steam-aging step. In contrast, V-maps increase in intensity, suggesting that V has migrated from the clay microporous structure onto the clay silicate layers (see Table 3).

The steam-aged rectorite sample in Fig. 4 has been scanned with an electron beam ~200 Å in diameter to generate a linescan spectrum for each particle examined. The linescan was performed on the particle side, thus it represents the true composition of the clay particles close to the layer's edges, Fig. 5. The linescan in Fig. 6 indicates that vanadium is spread out beyond the clay particle edges (left-hand side of curve). Some of the vanadium maxima match the structural elements (Al and Si), but Fe seems dispersed and independent of the structural elements. Isolated maxima of vanadium and Fe have been observed, indicating the presence of small islands of vanadium and Fe on the clay surface. Comparing linescans for the surface and for the edges, it appears that following steam-aging, V preferentially accumulates on the clay surface where it is somewhat uniformly distributed. (The scale factor in Fig. 5 is 5, whereas in Fig. 6, it is 6.)

HREM Results

Electron diffraction patterns for the rectorite sample under study consist of a series of rings which correspond to a sequence of *d*-spacings submultiple of (24.7 Å), the basal distance for allevardite (ASTM card 14-183) (*10*). After pillaring, the long-range, well-ordered stacking of silicate layers is retained (see Fig. 7). Lattice images indicate that, in general, this clay is indeed a 1 : 1 regular intrastratification of expandable and nonex-

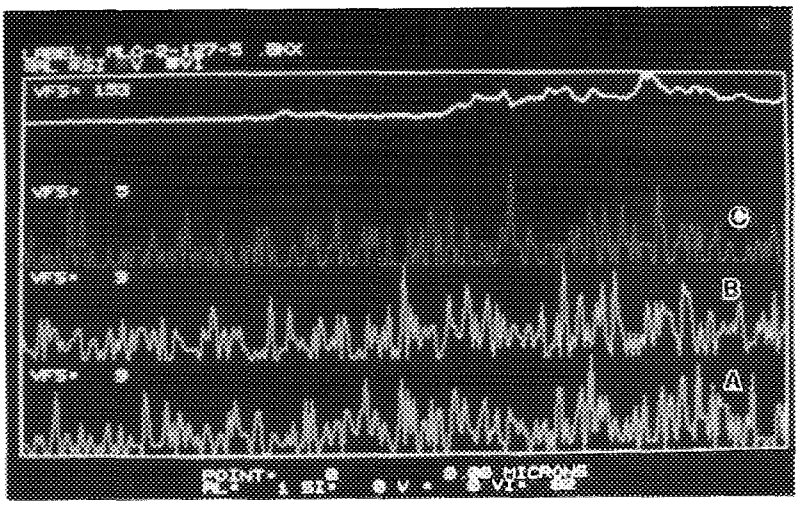

FIG. 5. Linescans of the edge of the rectorite plate in Figure 4 showing the distribution of (A) Al, (B) Si, and (C) V. The top line indicates the video contrast histogram.

pandable silicate layers (see Fig. 7). However, stacking disorders such as folded edges, twisted planes, bent planes, and multiple stacking of double layers (pyrophillite-like layers) have been observed in these samples (*10*). TEM micrographs for the ACH-rectorite (loaded with 1% V) after thermal and hydrothermal treatments are shown in Figs. 8 and 9, respectively. Calcination in air in the presence of 1% V did not seem to affect the clay pillared structure, and in agreement with XRD data, the basal spacing seemed to decrease slightly. HREM images in Fig. 8 show the preservation of the regular stacking sequence of montmorillonite-like and mica-like interspaces typical

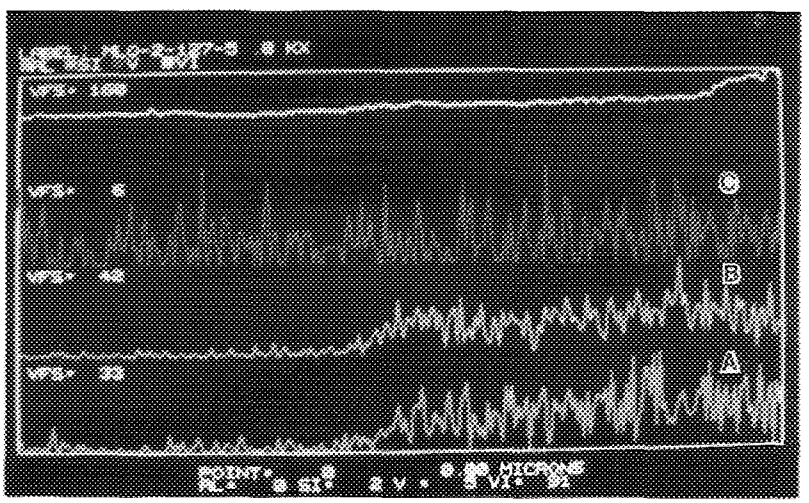

FIG. 6. Linescans of the (001) surface of the rectorite plate in Fig. 4 showing the distribution of (A) Al, (B) Si, and (C) V. The top line indicates the video contrast histogram.

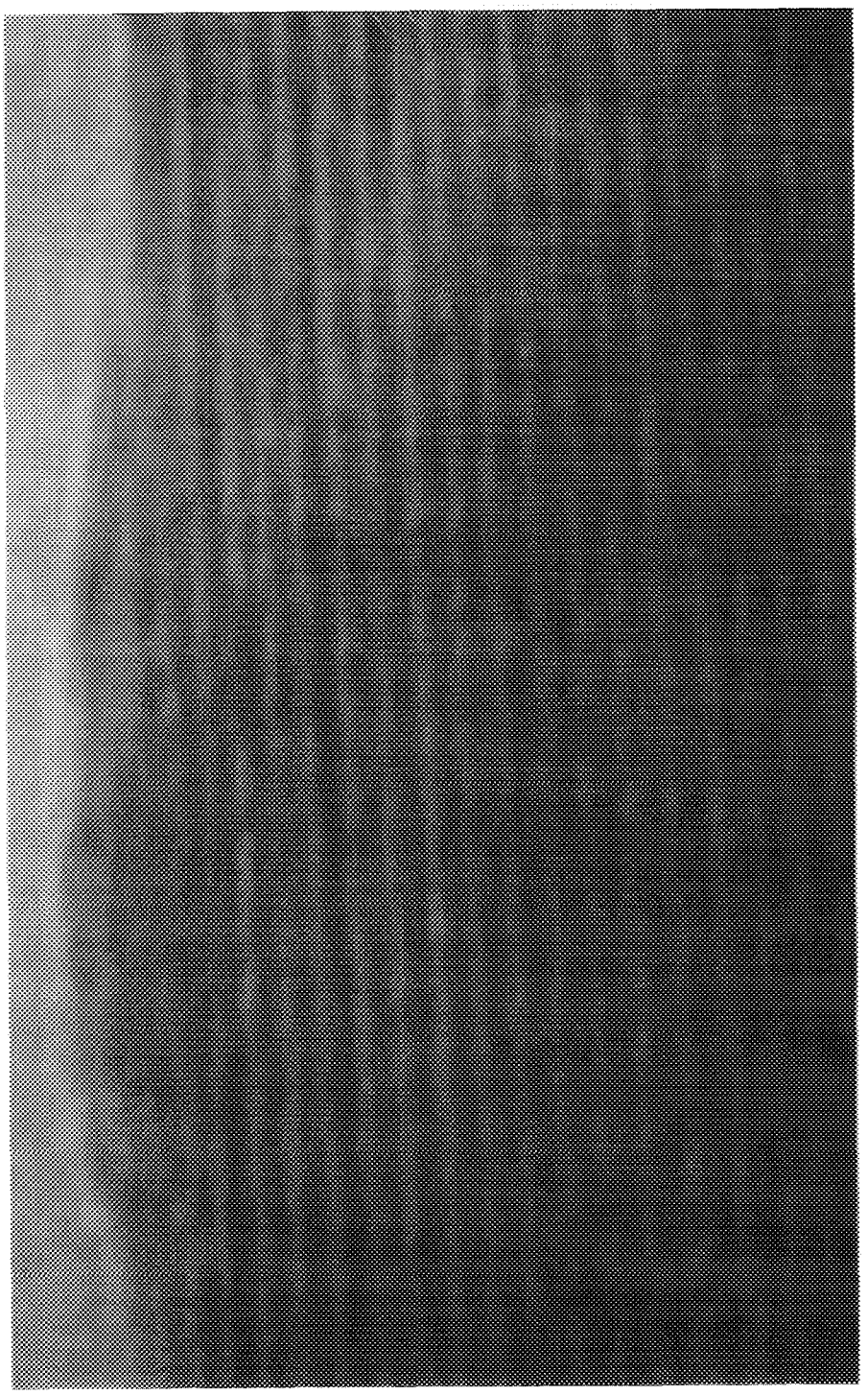

FIG. 7. TEM micrograph of the parent Mg-rectorite after expansion and pillaring with Al_{13}-ions. The sample has been dried in air at 400°C/10 h (1 cm = 52 Å).

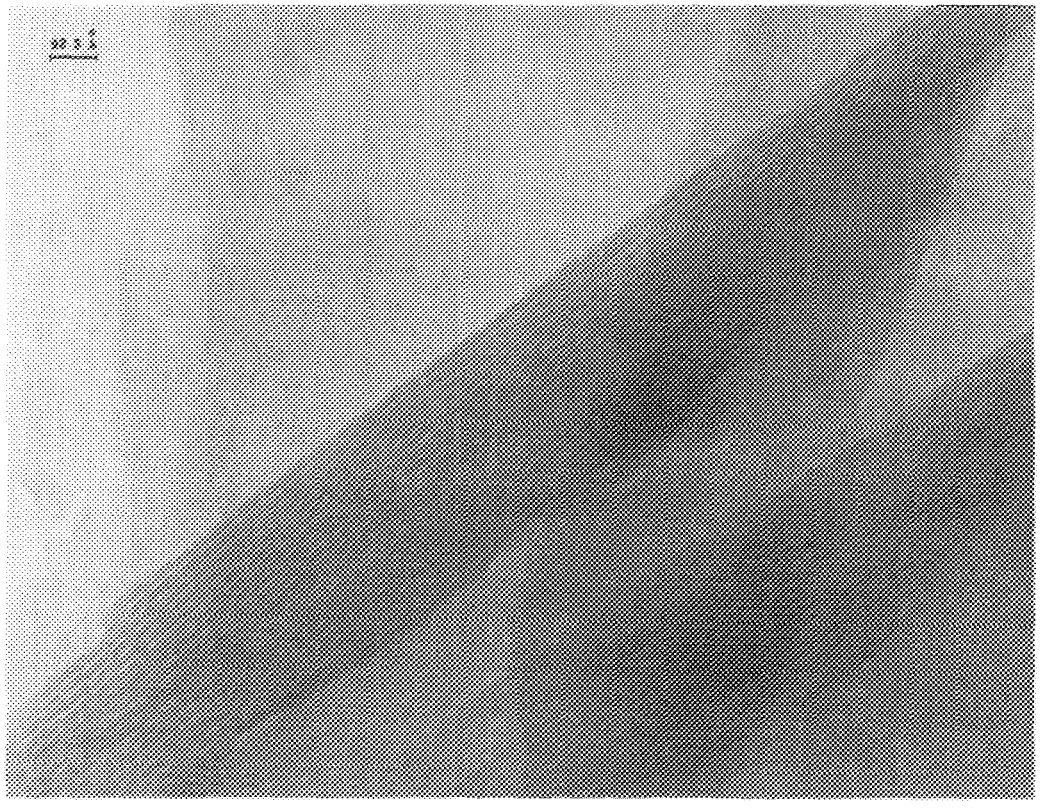

FIG. 8. TEM micrograph of the pillared rectorite after calcination in the presence of 1.0% V.

of these mixed-layer clays. Although some defects are present, layers remain straight and consequently, a uniform spacing of ~26 Å is observed (see Fig. 8). The calcined sample's crystallinity can be seen also in the corresponding optical transform (obtained in a laser optical bench) where a regular sequence of silicate layers along the [001] direction is observed. These results are well in agreement with X-ray diffraction results showing a sharp $d(001)$ reflection at 26.17 Å.

Steaming generates wavy planes and misorientation in the 1% V-loaded ACH–rectorite; amorphous patches (probably alumina) 20 to 90 Å in size appears (see Fig. 9). Furthermore, after steam-aging, partial (local) collapse of the pillared structure occurs, thus causing local variations in the interlayer space (see Fig. 9). The corresponding optical transforms (not shown) contain broad and extra spots along the [001] direction attributed to interplanar distance variations and to local rotation or twisting of the layers.

Vanadium 51-NMR Results

The ^{51}V NMR spectra of the calcined and steam-aged rectorites are summarized in Fig. 10. The vanadium-loaded rectorite samples were prepared by the incipient wetness impregnation technique using a solution of vanadyl naphthenate in benzene. Therefore, after drying (100°C/10 h in flowing air) all of the vanadium is located mainly into the clay microporous structure. Following the oxidative decomposition of the ligand, EDS indicates that some vanadium has migrated onto the clay surface (*10*), Tables 2 and 3. Thus, the ^{51}V NMR signals should arise

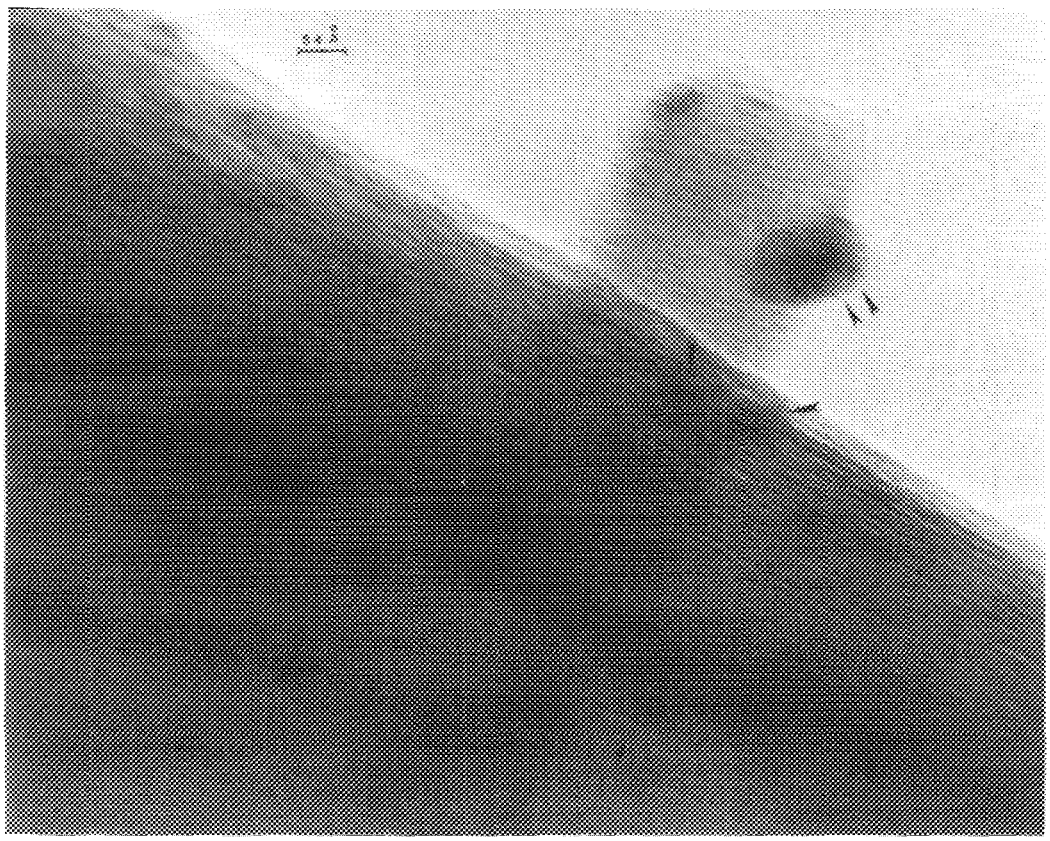

FIG. 9. TEM micrograph of the pillared rectorite after steam-aging in the presence of 1.0% V. Amorphous patches attributed to alumina debrids are indicated by arrows.

from vanadium species on the clay external surfaces as well as from V inside the clay microporous structure. The comparison of the ^{51}V NMR spectra in Fig. 10 reveals that pillaring the expandable layers in rectorite greatly influences the vanadium coordination. Figures 10A–10C show the results on the calcined-only samples. All three spectra can be explained in terms of two principal signal components with peak maxima near -300 and -680 ppm, respectively. The spectrum of the parent rectorite (where the -300 ppm peak is dominant) shows that this feature reflects a powder pattern defined by a near-to-axially symmetric anisotropic chemical-shift tensor with parallel and perpendicular components of -300 and -1250 ppm, respectively. These spectroscopic characteristics are typical for the distorted six-coordinated vanadium environment present in V_2O_5. Based on the dominance of this signal in the parent clay, this species is assigned to an amorphous or disordered V_2O_5 phase, formed on the outer surfaces of the rectorite crystals.

The feature near -680 ppm is tentatively assigned to four-coordinated vanadium (likely in a metavanadate- or pyrovanadate-like environment), as suggested by previous model compound studies (*7*, *9*). The spectra of this resonance resemble those of vanadium(V) oxide dispersed on alumina substrates (*7*, *8*). These results suggest that V-species interact intimately with the alumina pillars or with alumina debris resulting from partial pillar degradation during thermal and

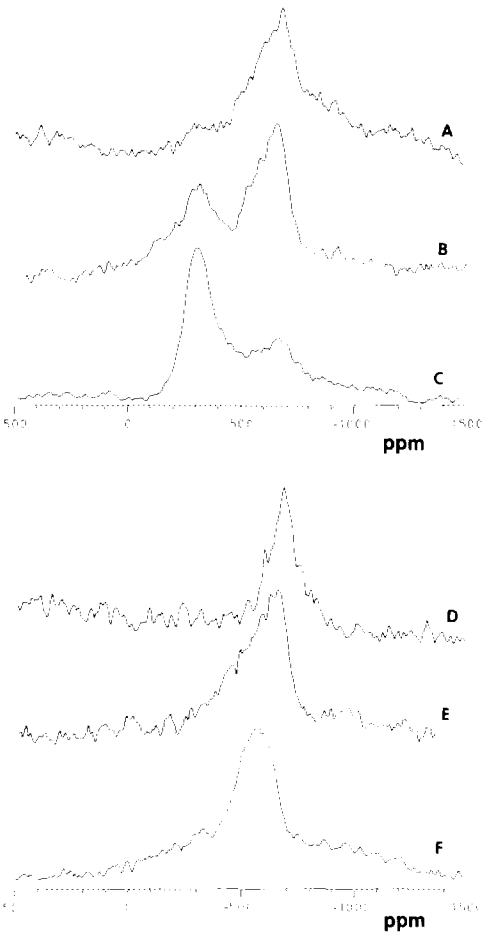

FIG. 10. 79.0-MHz ^{51}V solid-state NMR spectra of (A) pillared rectorite, 0.5 wt% V, calcined; (B) pillared rectorite, 1.0 wt% V, calcined; (C) parent rectorite, 1 wt% V, calcined; (D) pillared rectorite, 0.5 wt% V, calcined and steamed; (E) pillared rectorite, 1.0 wt% V, calcined and steamed; and (F) parent rectorite, 1.0 wt% V, calcined and steamed.

hydrothermal treatments. This signal makes the dominant contribution to the spectrum of the pillared rectorite loaded with 0.5 wt% V, while its contribution is decreased in the 1% V-pillared sample, and minimized in the parent rectorite loaded with 1% V. Based on these observations, this resonance is assigned to vanadia interacting with the aluminum oxide pillars inside the layers. The fact that this species also makes a small contribution to the spectrum of the parent sample (Fig. 10C) can possibly be explained by assuming that some VO^{2+} ions were exchanged into the rectorite-expandable layers during the impregnation step.

The above assignments and interpretations are reinforced by the spectra of the steam-aged samples shown in Figs. 10D–10F. For the sample containing 0.5 wt% V (Fig. 10D), the resonance position at -680 ppm remains unchanged, suggesting that the steam-aging treatment did not affect the vanadium environment. However, the sharper signal observed in the steam-aged sample suggests that the environment has become more uniform. In contrast, the parent rectorite loaded with 1 wt% V shows a pronounced change upon steaming, resulting in a new peak near -580 ppm (Fig. 10F). The formation of this new resonance can be attributed to the hydrolysis of the disordered vanadia phase on the rectorite surface with formation of polyvanadate species where vanadium is most likely four-coordinated (*4, 11–13*). As is the case for the calcined sample, the ^{51}V NMR spectrum for the steam-aged pillared rectorites loaded with 1 wt% V appears to be a superposition of the spectra shown in Figs. 10D and 10F. Thus, in the 1% V pillared sample, part of the vanadium still interacts with alumina species (either inside or outside the expandable layers) and part of the vanadium is present in the form of a polyvanadate species remote from the alumina present. This result is consistent with the XRD data, indicating partial collapse of the pillared layer structure at this loading and with EDS data indicating partial migration of vanadium to the surface.

Figure 11 shows the effect of surface dehydration (1 h, 200°C, 10^{-3} Torr) on the ^{51}V NMR spectra of the pillared rectorite loaded with 1 wt% V. The spectra indicate the disappearance of both the -300-ppm peak and the -580-ppm peak in the calcined and steamed samples, respectively. This result illustrates that the site distinction possible in Figs. 10A–10F is related to the presence of hydrous surface species (OH, H_2O),

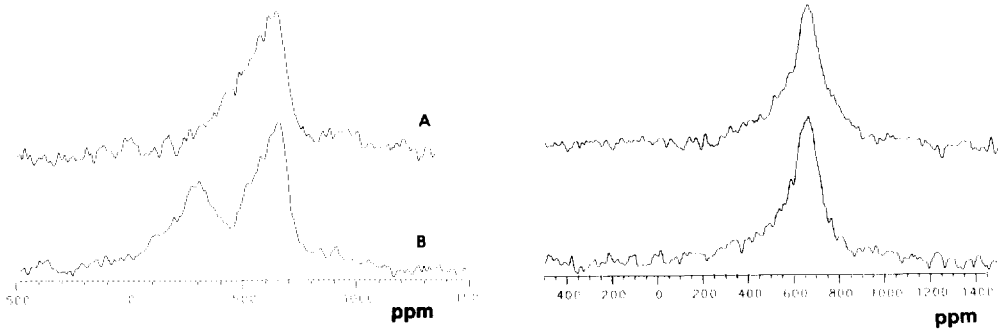

FIG. 11. 79.0-MHz ^{51}V solid-state NMR spectra of (A) pillared rectorite with 1% V, calcined and (B) pillared rectorite with 1% V calcined and steamed. Left side: ambient samples. Right side: samples dehydrated at about 200°C in a 10^{-3} Torr vacuum.

which participate in the coordination environments of those vanadium atoms present on the external clay surface. In contrast, no clear site discrimination is possible in the dehydrated state, where all of the vanadium appears to be four-coordinated. Thus, surface water appears to enhance the chemical shift distinction between subtly different vanadium(V) oxide environments by modifying and/or expanding the vanadium coordination spheres. To monitor the fate of the vanadium species during the various thermal and hydrothermal steps, it is therefore important to study the pillared rectorite catalysts under ambient conditions.

CONCLUSIONS

In the presence of 0.5–1.0% V, the thermal and hydrothermal stability at MAT conditions of rectorites pillared with alumina clusters is similar to that of a commercially available FCC containing an estimated 35% CREY. Microprobe analysis has indicated that after steam-aging, V migrates to the crystal's outer surface. At 1% V, steaming causes the decomposition of the alumina pillars and the catalyst surface area decreases to 18 m^2/g from 147 m^2/g. XRD and TEM results suggest that after the pillar decomposition, the rectorite partially retains its face-to-face connection of silicate layers. The presence of wavy planes and misorientation of the clay layers in the steam-aged samples have been indicated by HREM results. Layer rigidity is believed responsible for the pillared rectorite's exceptional hydrothermal stability at 760°C.

Solid-state ^{51}V NMR spectroscopy is a powerful technique to monitor the effect of V-loading, pillaring, and steam-aging, and surface-dehydration on the local vanadium coordination environments. In particular, the ^{51}V spectra of the hydrated clay differentiate sensitively between the vanadia species on the internal and external surfaces, thus allowing monitoring of the process of pillar decomposition and structural collapse.

ACKNOWLEDGMENTS

The support received by MLO from the Unocal Analytical Department staff is gratefully acknowledged. Special thanks are due to Mr. M. Bell and Ms. E. Rivette for XRD data and for many useful discussions. This work was supported by NSF Grant DMR-89-13738 to H.E.

REFERENCES

1. Guan, J., Min, E., and Yu, Z., European Patent Application 0197012 (1986).
2. Guan, J., Min, E., and Yu, Z., *in* "Proceedings of the 9th International Congress on Catalysis, Calgary, 1988" (M. J. Phillips and M. Ternan, Eds.), Vol. 1, pp. 104–111. Chem. Inst. Canada, Ottawa, 1988.
3. Occelli, M. L., *in* "Scientific Bases Prep. Heterog. Catalysts, 5th Int. Symposium" (G. Poncelet,

P. A. Jacobs, P. Grange, B. Delmon, Eds.) p. 287. 1991.
4. Occelli, M. L., *Catal. Rev.* **33,** 241 (1991).
5. Occelli, M. L., Stencel, J. M., and Suib, S. L., *in* "Chemistry of Microporous Crystals" (T. Inui, S. Namba, and T. Tatsumi, Eds.), p. 353. Kodansha, Tokyo, 1991.
6. Mitchell, B. R., *Ind. Eng. Chem. Prod. Res. Dev.* **19,** 209 (1980).
7. Occelli, M. L., Dominguez, J. M., and Eckert, H., Paper presented at the California Catalysis Society Meeting, Richmond, CA, April 25, 1991.
8. Eckert, H., and Wachs, I. E., *J. Phys. Chem.* **93,** 6796 (1989).
9. Eckert, H., and Wachs, I. E., *Mater. Res. Soc. Symp. Proc.* **111,** 455 (1988).
10. Iyer P. S., Eckert, H., Occelli, M. L., and Stencel, J. M. *in* "Fluid Catalytic Cracking II: Concepts in Catalyst Design" (M. L. Occelli, Ed.), ACS Symposium Series, Vol. 452, p. 242. Am Chem. Soc., Washington, DC, 1991.
11. Dominguez, J. M., and Occelli, M. L., *in* "Symp. on Zeolites and Pillared Clay Synthesis, New York, August 24, 1991," in press.
12. Pope, M. T., and Dale, B. W., *Rev. (London)* **22,** 527 (1968).
13. O'Donnell, S. E., and Pope, M. T., *J. Chem. Soc. Dalton Trans.*, 21 (1976).